Phonon-Driven Ultrafast Exciton Dissociation at Donor-Acceptor Polymer Heterojunctions

Hiroyuki Tamura,[1] John G. S. Ramon,[2] Eric R. Bittner,[2] and Irene Burghardt[1]

[1]*Département de Chimie, Ecole Normale Supérieure, 24 rue Lhomond, F–75231 Paris cedex 05, France*

[2]*Department of Chemistry and Texas Center for Superconductivity, University of Houston, Houston, Texas 77204, USA*

(Received 13 June 2007; published 12 March 2008)

A quantum-dynamical analysis of exciton dissociation at polymer heterojunctions is presented, using a hierarchical electron-phonon model parametrized for three electronic states and 28 vibrational modes. Two representative interfacial configurations are considered, both of which exhibit an ultrafast exciton decay. The efficiency of the process depends critically on the presence of intermediate bridge states, and on the dynamical interplay of high- vs low-frequency phonon modes. The ultrafast, highly nonequilibrium dynamics is consistent with time-resolved spectroscopic observations.

DOI: 10.1103/PhysRevLett.100.107402 PACS numbers: 78.55.Kz, 63.22.−m, 71.20.Rv, 71.35.−y

Semiconducting π-conjugated polymers are promising low-cost and flexible materials for electronic devices such as organic light-emitting diodes (OLEDs) and solar cells [1–3]. Many of the unique properties of these materials stem from the combination of the molecular structure of their building blocks and the extended nature of the π system. Thus, excitonic states, i.e., electron-hole quasiparticle states that extend over the polymer strands, play a central role for the optoelectronic properties [3]. Exciton formation can result from polaron recombination, e.g., in OLEDs, or else from the primary photoexcitation step, e.g., in photovoltaic systems.

A key feature of organic semiconductors is the strong coupling between the elementary electronic processes and the material's phonon modes [3,4]—much stronger than in inorganic semiconductors. This is underscored by experimental observations of subpicosecond scale coherent nuclear motions following photoexcitation [5]. Further, the ultrafast nature of the electronic decay processes [6–8] suggests the presence of coherent vibronic coupling mechanisms, possibly determined by conical intersection topologies—very similar to the photophysics of polyatomic molecules and to Jahn-Teller effects in solids [9]. These observations call for a microscopic-level, quantum-dynamical interpretation of the basic charge- and energy-transfer processes.

In this Letter, we focus on the role of electron-phonon coupling in the charge-transfer processes at bulk polymer heterojunctions [10]; these provide conditions for an extremely efficient charge separation at the interface between different phase-segregated polymers. The primary excitation is a photogenerated exciton stabilized by the electron-hole Coulombic interaction (with a typical binding energy of $\epsilon_B \sim 0.5$ eV [2]). Because of the highly folded interfacial area in bulk heterojunctions, the exciton has a high probability of reaching the interface within the diffusion length (typically ~20 nm). The exciton decay towards a charge-separated state ("exciplex") is largely determined by molecular-level electronic interactions at the interface. To a first approximation, the efficiency of charge generation depends on the ratio between ϵ_B and the band offset between the two polymer species [10,11]. Recent time-resolved photoluminescence studies have shown that the exciton decay—and possible exciton regeneration—fall into a (sub)picosecond regime [7,8]. While the elementary processes at the polymer interface are crucial for the device function and optimization, these processes are not well characterized as yet on the microscopic side. Against this background, we propose a strategy which combines a molecular-level electronic structure and quantum-dynamical characterization of the system with a sampling over the relevant interface configurations.

We specifically consider a heterojunction composed of the poly[9, 9-dioctylfluorene-co-*N*-(4-butylphenyl)diphenylamine] (TFB) and poly[9,9-dioctylfluorene-co-benzothiadiazole] (F8BT) polymer components [7,11]. At the TFB:F8BT heterojunction, ϵ_B is found to be similar to the band offset, so that both exciton decay and regeneration phenomena are expected to occur. Semiempirical calculations were used to identify the relevant electronic states and parametrize the vibronic coupling Hamiltonian used below [see Eq. (1)] for 28 explicit

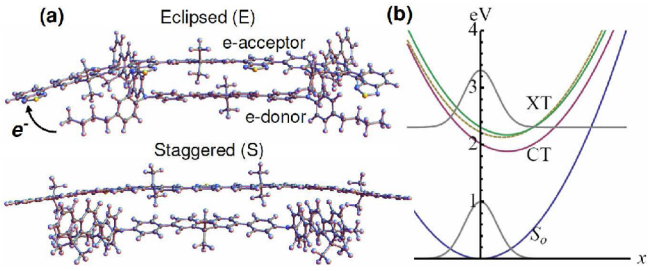

FIG. 1 (color online). Schematic illustration of (a) the eclipsed vs staggered configurations of the TFB:F8BT donor-acceptor heterojunction under study and (b) the photoexcitation process and potential crossings, involving the XT (green or gray), CT (mauve or dark gray), and IS (ochre or light gray) states. The minima and Franck-Condon (vertical) energies correspond to the computed adiabatic (relaxed) and vertical excitation energies, respectively, for the E configuration.

phonon modes covering the high-frequency (C=C stretch) and low-frequency (ring-torsional) phonon branches [11–13]. Two representative interface structures are investigated, i.e., an eclipsed (E) configuration with π-stacked fluorene units and a staggered (S) configuration with laterally displaced chains [14], see Fig. 1. For the E configuration, single-particle interchain hopping terms were included [11], while these were assumed to be absent in the S configuration. The exciton state (XT), which is the lowest excited state with significant oscillator strength, mainly has electron-hole density on the F8BT moiety, while the lowest-lying interfacial charge-transfer state (CT) corresponds to a TFB^+-$F8BT^-$ charge-separated state [15]. Among the manifold of remaining states, one is found to exhibit a strong coupling to the XT state [12]; this higher-lying charge-transfer state will be considered as an intermediate state (IS) in the following. Recent experimental studies provide strong indications that such an intermediate state could play a crucial role in the photocurrent generation [7].

To interpret the nonadiabatic decay of the exciton state, we apply a three-state vibronic coupling model in conjunction with highly accurate wave packet propagation techniques, i.e., the multiconfiguration time-dependent Hartree (MCTDH) method [16]. In particular, we use a linear vibronic coupling (LVC) model [9] which is appropriate in view of the moderate nuclear displacements during the process. The N-mode LVC Hamiltonian (here, $N = 28$) reads as follows, using mass and frequency weighted coordinates and atomic units ($\hbar = 1$),

$$\boldsymbol{H} = \sum_{i=1}^{N} \frac{\omega_i}{2}(p_i^2 + x_i^2)\mathbf{1} + \sum_{i=1}^{N} \begin{pmatrix} \kappa_i^{(1)} x_i & \lambda_i^{(12)} x_i & \lambda_i^{(13)} x_i \\ \lambda_i^{(12)} x_i & \kappa_i^{(2)} x_i & \lambda_i^{(23)} x_i \\ \lambda_i^{(13)} x_i & \lambda_i^{(23)} x_i & \kappa_i^{(3)} x_i \end{pmatrix} + \boldsymbol{C}. \quad (1)$$

Here, $\mathbf{1}$ and $\boldsymbol{C}$ denote the unit matrix and a coordinate independent constant matrix, respectively; the ω_i, $p_i = -i\partial/\partial x_i$, and x_i are the frequencies, momenta, and displacements along the vibrational normal modes. The diagonal and off-diagonal potential terms correspond to the diabatic potentials and couplings. The model Eq. (1) allows for the presence of conical intersections between pairs of electronic states at nuclear configurations where the diabatic coupling vanishes and the adiabatic states become degenerate [9]. The E vs S configurations generate significantly different model parametrizations [17], pertaining to a strong-coupling vs weak-coupling regime, respectively.

We further apply a recently developed effective-mode representation of the LVC model [18], which separates the Hamiltonian into effective-mode vs residual-mode parts,

$$\boldsymbol{H} = \boldsymbol{H}_{\text{eff}} + \boldsymbol{H}_{\text{res}}. \quad (2)$$

By an orthogonal coordinate transformation, $\boldsymbol{X} = \boldsymbol{T}\boldsymbol{x}$, a subset of effective modes is generated which subsume all vibronic coupling terms of an electronic N_s-state system into $\frac{1}{2}N_s(N_s+1)$ effective modes [18]. This construction, which was previously applied to two-state systems (three effective modes) [13,18,19], is here extended to three electronic states (six effective modes),

$$\boldsymbol{H}_{\text{eff}} = \sum_{i=1}^{6} \frac{\Omega_i}{2}(P_i^2 + X_i^2)\mathbf{1} + \sum_{i=1}^{6} \begin{pmatrix} (K_i + D_i)X_i & \Lambda_i^{(12)} X_i & \Lambda_i^{(13)} X_i \\ \Lambda_i^{(12)} X_i & (K_i - D_i)X_i & \Lambda_i^{(23)} X_i \\ \Lambda_i^{(13)} X_i & \Lambda_i^{(23)} X_i & K_i^{(3)} X_i \end{pmatrix} + \sum_{i=1}^{6} \sum_{j=i+1}^{6} d_{ij}(P_i P_j + X_i X_j)\mathbf{1} + \boldsymbol{C}, \quad (3)$$

where the parameters and modes $\boldsymbol{X}$ are defined by extension of the two-state construction described in Refs. [13,18]. Two of the six effective modes (i.e., X_1 and X_2) are chosen as topology-adapted modes which span the branching plane [9,18] for a given pair of electronic states (here, states 1 and 2), i.e., the plane along which the degeneracy at the conical intersection is lifted, see Fig. 2. Several of the coupling constants in Eq. (3), i.e., the $\Lambda_i^{(12)}$ ($i \geq 2$), D_i ($i \geq 3$), K_i ($i = 4, 5, 6$), $\Lambda_i^{(13)}$ ($i = 5, 6$), and $\Lambda_6^{(23)}$, are zero by construction.

The residual modes, X_i, $i = 7, \ldots, N$, do not couple directly to the electronic subsystem, but couple bilinearly to the effective modes. By analogy with our recent two-state analysis [13], $\boldsymbol{H}_{\text{res}}$ can be transformed to a band-diagonal structure, yielding the nth-order Hamiltonian

$$\boldsymbol{H}^{(n)} = \boldsymbol{H}_{\text{eff}} + \sum_{l=1}^{n} \boldsymbol{H}_{\text{res}}^{(l)}, \quad (4)$$

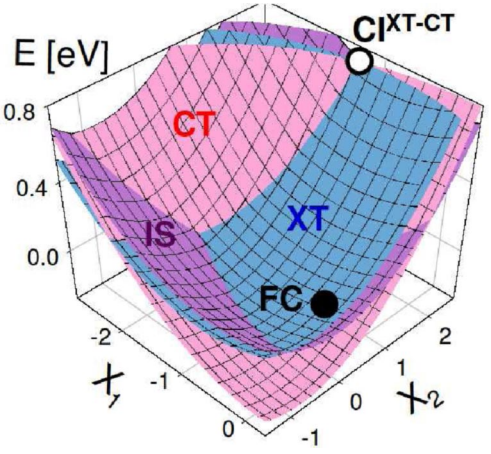

FIG. 2 (color online). Projections of the coupled diabatic XT, CT, and IS PESs (E configuration) onto the XT-CT branching plane. The white and black circles indicate the conical intersection and Franck-Condon geometry, respectively.

where each lth-order residual term comprises 6 modes,

$$\boldsymbol{H}_{\mathrm{res}}^{(l)} = \sum_{i=6l+1}^{6l+6} \frac{\Omega_i}{2}(P_i^2 + X_i^2)\mathbf{1} + \sum_{i=6l+1}^{6l+6} \sum_{j=i-6}^{i-1} d_{ij}(P_i P_j + X_i X_j)\mathbf{1}. \tag{5}$$

For $6 + 6n = N$, the nth-order Hamiltonian $\boldsymbol{H}^{(n)}$ is equivalent to the original Hamiltonian Eq. (1).

We refer to Eqs. (2) and (3) in conjunction with Eqs. (4) and (5) as a hierarchical electron-phonon (HEP) model [13,19]. Successive orders $\boldsymbol{H}^{(n)}$ of the HEP Hamiltonian can be shown to conserve the moments (cumulants) of the original Hamiltonian up to the $(2n + 3)$rd order [13]. Truncation of the HEP Hamiltonian creates a series of reduced-dimensionality models, associated with approximate nth-order propagators which accurately reproduce the dynamics of the overall system up to a certain time. Whether or not $\boldsymbol{H}_{\mathrm{eff}}$ by itself can account for the ultrafast exciton decay depends on the diabatic coupling strength and local topology. In our previous analysis of a two-state XT-CT model [13], the HEP construction had to be taken to the order $\boldsymbol{H}^{(1)}$ to obtain a qualitatively correct description. While $\boldsymbol{H}_{\mathrm{eff}}$ turns out to be essentially determined by high-frequency C═C stretch modes which dominate the coupling to the electronic subsystem, $\boldsymbol{H}_{\mathrm{res}}^{(1)}$ is composed of low-frequency ring-torsional modes; these latter modes have been shown to play a crucial role in producing the ultrafast exciton decay [13].

Figure 2 shows the diabatic XT, CT, and IS potential energy surfaces (PES) of the E configuration, for a cut through the XT-CT branching plane defined in terms of the effective modes (X_1, X_2). As can be inferred from the figure, the exciton dissociation process is determined by a landscape of multiple intersecting surfaces, and the branching plane topology is a key factor in the nonadiabatic dynamics. Of particular interest for the present analysis is the role of the intermediate state (IS) that could mediate the exciton decay.

Figure 3(a) shows the population evolution obtained from MCTDH simulations for the overall 3-state, 28-mode system (E configuration) according to Eq. (1). An ultrafast initial XT → CT decay takes place (~50% at 100 fs), followed by an oscillatory behavior of the XT, CT, and IS populations which is found to persist over a 0.5 ps interval. A steady increase of both the CT and IS populations is observed. An analogous simulation for the S configuration [Fig. 3(c)] also shows a subpicosecond decay, even though on a somewhat slower time scale; here, the IS population always remains small. Given that the S configuration features significantly weaker couplings ($\Lambda_1^{(12)} \simeq 0.005$ eV) than the E configuration ($\Lambda_1^{(12)} \simeq 0.04$ eV), the fast XT decay may appear surprising.

To investigate the respective roles of the direct (XT → CT) vs indirect (bridge-mediated) pathways, we have carried out complementary simulations that were restricted to the two-state XT-CT subspace [Figs. 3(b) and 3(d)]. These show for both the E and S configurations that a much less pronounced XT decay is observed in the absence of the IS state [20]. Hence, the efficient exciton dissociation of Figs. 3(a) and 3(c) is to a significant extent due to the indirect XT → IS → CT pathway; that is, the IS state mediates the charge separation (while also acting as a competing final state). That an ultrafast decay is observed for both the E and S structures suggests that the exciton decay is dynamically robust [21]. Despite the marked differences in the spectroscopy of the E vs S configurations [14], the dynamical signatures are apparently similar.

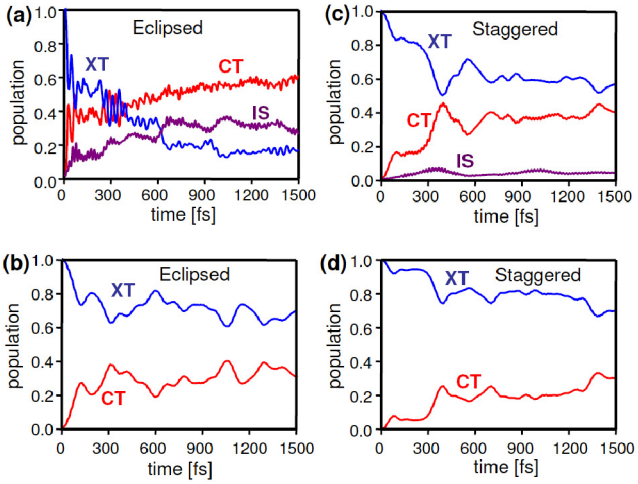

FIG. 3 (color online). Time-evolving state populations for (a) the full 3-state 28-mode wave packet propagation for the E configuration, and (b) a complementary 2-state 28-mode calculation for the E configuration that was restricted to the XT-CT subspace; (c) and (d) are analogous calculations for the S configuration.

The remaining part of the analysis addresses the HEP construction of Eqs. (2)–(5), with the twofold objective of identifying a reduced-dimensionality picture of the dynamics and understanding the role of the different types of phonon modes, i.e., high-frequency C═C stretch modes (constituting $\boldsymbol{H}_{\mathrm{eff}}$) vs low-frequency ring-torsional modes (constituting $\boldsymbol{H}_{\mathrm{res}}^{(1)}$). As shown in Fig. 4, the high-frequency modes by themselves, at the level of the 6-mode $\boldsymbol{H}^{(0)} = \boldsymbol{H}_{\mathrm{eff}}$ model, give a better approximation of the dynamics for the E configuration (strong-coupling case) than for the S configuration (weak-coupling case). Inclusion of the low-frequency modes, at the level of the 12-mode $\boldsymbol{H}^{(1)}$ approximation, results in a qualitatively correct description in both cases. Finally, the $\boldsymbol{H}^{(2)}$, 18-mode approximation is essentially identical to the full-dimensional, 28-mode result on a ~1 ps time scale. The HEP analysis underlines that the high-frequency modes dominate the coherent short-time dynamics while the low-frequency modes induce energy redistribution and dephasing [13]. The present observations point to the generic nature of this pattern for

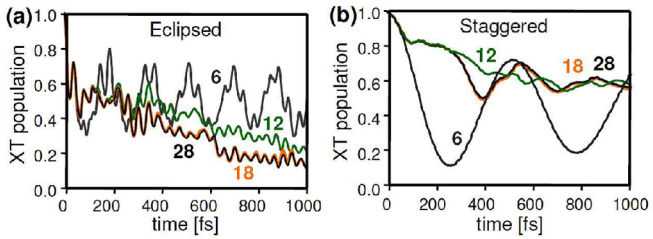

FIG. 4 (color online). Time-evolving XT population for the truncated HEP Hamiltonian $\mathbf{H}^{(n)}$ of Eq. (4), for $n = 0$ (6 modes), $n = 1$ (12 modes), and $n = 2$ (18 modes), as compared with the full-dimensional 28-mode result, for both the E (left-hand side) and S (right-hand side) configurations [22].

the characteristic two-band phonon distribution. All of these results would carry over to an initial parametrization involving a very large number N of phonon modes, e.g., thousands of modes. While dynamical calculations according to Eq. (1) would not be feasible for such a "macrosystem," the HEP model gives a correct reduced-dimensionality description of the ultrafast dynamics.

In summary, we present the results of fully quantum-dynamical calculations of a model polymer heterojunction interface, for two representative interface configurations that generate distinct supermolecular systems. These results highlight that it is essential to (i) analyze an ensemble of interface structures, in keeping with the observations of Refs. [8,14] and (ii) include intermediate states in a minimal model of the heterojunction. While the transfer efficiency at individual avoided-crossing (or conical intersection) topologies can depend in a sensitive fashion on the molecular polymer structure, we conjecture that the dynamical robustness of the ultrafast decay results from the presence of multiple decay pathways. The present approach should contribute to a realistic modeling of the ultrafast energy and charge-transfer processes in extended systems, and provide new criteria for material design.

We thank Andrey Pereverzev, Etienne Gindensperger, and Lorenz Cederbaum for useful discussions. This work was supported by Projects No. ANR-05-NANO-051-02 and No. ANR-NT05-3-42315, by NSF Grant No. CHE-0345324, and by the Robert Welch Foundation. E. R. B. gratefully acknowledges support from the John S. Guggenheim Foundation.

[1] R. H. Friend *et al.*, Nature (London) **397**, 121 (1999); J. L. Brédas, D. Beljonne, V. Coropceanu, and J. Cornil, Chem. Rev. **104**, 4971 (2004); S. Günes, H. Neugebauer, and N. S. Sariciftci, Chem. Rev. **107**, 1324 (2007).
[2] J. J. M. Halls *et al.*, Phys. Rev. B **60**, 5721 (1999).
[3] G. D. Scholes and G. Rumbles, Nat. Mater. **5**, 683 (2006).
[4] S. Tretiak, A. Saxena, R. L. Martin, and A. R. Bishop, Phys. Rev. Lett. **89**, 097402 (2002).
[5] G. Lanzani, G. Cerullo, C. Brabec, and N. S. Sariciftci, Phys. Rev. Lett. **90**, 047402 (2003).
[6] R. Kersting *et al.*, Phys. Rev. Lett. **70**, 3820 (1993).
[7] A. C. Morteani *et al.*, Phys. Rev. Lett. **92**, 247402 (2004).
[8] P. Sreearunothai *et al.*, Phys. Rev. Lett. **96**, 117403 (2006).
[9] H. Köppel, W. Domcke, and L. S. Cederbaum, Adv. Chem. Phys. **57**, 59 (1984); *Conical Intersections*, edited by W. Domcke, D. R. Yarkony, and H. Köppel (World Scientific, NJ, 2004), Vol. 15.
[10] G. Yu *et al.*, Science **270**, 1789 (1995); J. J. M. Halls *et al.*, Nature (London) **376**, 498 (1995).
[11] E. R. Bittner, J. G. S. Ramon, and S. Karabunarliev, J. Chem. Phys. **122**, 214719 (2005); E. R. Bittner and J. G. S. Ramon, in *Quantum Dynamics of Complex Molecular Systems*, edited by D. A. Micha and I. Burghardt, Springer Series in Chemical Physics Vol. 83 (Springer, Heidelberg, 2007).
[12] J. G. S. Ramon and E. R. Bittner, J. Phys. Chem. B **110**, 21001 (2006).
[13] H. Tamura, E. R. Bittner, and I. Burghardt, J. Chem. Phys. **126**, 021103 (2007); **127**, 034706 (2007).
[14] J. G. S. Ramon and E. R. Bittner, J. Chem. Phys. **126**, 181101 (2007).
[15] However, the CT state of the E configuration is not purely polaronic since it does carry oscillator strength to the ground state through mixing with excitonic configurations on the F8BT moiety.
[16] H.-D. Meyer, U. Manthe, and L. S. Cederbaum, Chem. Phys. Lett. **165**, 73 (1990); M. H. Beck, A. Jäckle, G. A. Worth, and H.-D. Meyer, Phys. Rep. **324**, 1 (2000); G. A. Worth *et al.*, The MCTDH Package, Version 8.3, see http://www.pci.uni-heidelberg.de/tc/usr/mctdh/.
[17] See EPAPS Document No. E-PRLTAO-100-072809 for a list of parameters pertaining to the E vs S configurations, respectively, for the 3-state 28-mode model Eq. (1). For more information on EPAPS, see http://www.aip.org/pubservs/epaps.html.
[18] L. S. Cederbaum, E. Gindensperger, and I. Burghardt, Phys. Rev. Lett. **94**, 113003 (2005); E. Gindensperger, I. Burghardt, and L. S. Cederbaum, J. Chem. Phys. **124**, 144103 (2006); I. Burghardt, E. Gindensperger, and L. S. Cederbaum, Mol. Phys. **104**, 1081 (2006).
[19] E. Gindensperger, H. Köppel, and L. S. Cederbaum, J. Chem. Phys. **126**, 034106 (2007).
[20] This is in contrast to our previous 2-state analysis [13], and can be attributed to differences in the PES topology which is a sensitive function of the interface structure.
[21] While we have found that small parameter variations can effectively inhibit the XT decay within the two-state XT-CT model, an efficient decay is always observed in the presence of bridge states.
[22] Note that the 28-mode trace is slightly different from Fig. 3 beyond 400 fs, due to the fact that the calculations relate to different representations of the Hamiltonian and are not fully converged.